SIAM J. Applied Dynamical Systems
Vol. 7, No. 4, pp. 1355–1377

Singular Hopf Bifurcation in Systems with Two Slow Variables*

John Guckenheimer†

Abstract. Hopf bifurcations have been studied intensively in two dimensional vector fields with one slow and one fast variable [É. Benoît et al., *Collect. Math.*, 31 (1981), pp. 37–119; F. Dumortier and R. Roussarie, *Mem. Amer. Math. Soc.*, 121 (577) (1996); W. Eckhaus, in *Asymptotic Analysis* II, Lecture Notes in Math. 985, Springer-Verlag, Berlin, 1983, pp. 449–494; M. Krupa and P. Szmolyan, *SIAM J. Math. Anal.*, 33 (2001), pp. 286–314; J. Guckenheimer, in *Normal Forms, Bifurcations and Finiteness Problems in Differential Equations*, NATO Sci. Ser. II Math. Phys. Chem. 137, Kluwer, Dordrecht, The Netherlands, 2004, pp. 295–316]. *Canard explosions* are associated with these *singular Hopf* bifurcations [S. M. Baer and T. Erneux, *SIAM J. Appl. Math.*, 46 (1986), pp. 721–739; S. M. Baer and T. Erneux, *SIAM J. Appl. Math.*, 52 (1992), pp. 1651–1664; B. Braaksma, *J. Nonlinear Sci.*, 8 (1998), pp. 457–490; Y. Lijun and Z. Xianwu, *J. Differential Equations*, 206 (2004), pp. 30–54], manifested by a very rapid growth in the amplitude of periodic orbits. There has been less analysis of Hopf bifurcations in slow-fast systems with two slow variables where singular Hopf bifurcation occurs simultaneously with *type* II *folded saddle-nodes* [A. Milik and P. Szmolyan, in *Multiple-Time-Scale Dynamical Systems*, IMA Vol. Math. Appl. 122, Springer-Verlag, New York, 2001, pp. 117–140; M. Wechselberger, *SIAM J. Appl. Dyn. Syst.*, 4 (2005), pp. 101–139]. This work contributes to our understanding of these Hopf bifurcations in five ways: (1) it computes the first Lyapunov coefficient of the bifurcation in terms of a normal form, (2) it describes global features of the flow that constrain the types of trajectories found in the system near the bifurcation, (3) it identifies codimension two bifurcations that occur as coefficients in the normal form vary, (4) it exhibits complex solutions that occur in the vicinity of the bifurcation for some values of the normal form coefficients, and (5) it identifies singular Hopf bifurcation as a mechanism for the creation of mixed-mode oscillations. A subtle aspect of the normal form is that terms of higher order contribute to the first Lyapunov coefficient of the bifurcation in an essential way.

Key words. Hopf bifurcation, mixed mode oscillation, singular perturbation

AMS subject classifications. 37M20, 34E13, 37G10

DOI. 10.1137/080718528

1. Introduction.

Slow-fast vector fields have the form

$$\begin{aligned} \varepsilon \dot{x} &= f(x, y, \varepsilon), \\ \dot{y} &= g(x, y, \varepsilon), \end{aligned} \tag{1.1}$$

with $x \in R^m$ as the fast variable, $y \in R^n$ as the slow variable, and ε as a small parameter that represents the ratio of time scales. The set of points satisfying $f = 0$ is the *critical manifold* of the system: slow motion of trajectories can occur only near the critical manifold. Fenichel theory [14] establishes that there are invariant slow manifolds of the system near portions of the critical manifold, where $D_x f$ is hyperbolic. Moreover, the trajectories on the

*Received by the editors March 14, 2008; accepted for publication (in revised form) by T. Kaper July 10, 2008; published electronically October 31, 2008.
http://www.siam.org/journals/siads/7-4/71852.html
†Mathematics Department, Cornell University, Ithaca, NY 14853 (jmg16@cornell.edu).

slow manifold approach trajectories of the *slow flow* $\dot{y} = g(h(y), y, 0)$ on the critical manifold where h is defined implicitly by $f(h(y), y, 0) = 0$. Points of the critical manifold where $D_x f$ is singular are called *fold* points. In much of the literature on slow-fast models of neural systems, the fold points are called "knees" [29].

Hopf bifurcation occurs in the following slow-fast system with one slow and one fast variable:

$$\begin{aligned} \varepsilon \dot{x} &= y - x^2/2 - x^3/3, \\ \dot{y} &= \mu - x. \end{aligned} \tag{1.2}$$

This system has an equilibrium point at $(\mu, \mu^2/2 + \mu^3/3)$ that undergoes a supercritical Hopf bifurcation as μ decreases through zero. The Hopf equilibrium is at the fold of the system. We also note that the slow flow along the critical manifold has a stable equilibrium on a stable branch of the critical manifold for $\mu > 0$ but an unstable equilibrium on the unstable branch of the critical manifold for $-1 < \mu < 0$. The periodic orbits that emerge from the Hopf bifurcation grow explosively from an amplitude that is $O(\varepsilon^{1/2})$ to an amplitude that is $O(1)$ over a range of values of μ that has length $O(\exp(-c/\varepsilon))$ for a constant $c > 0$ independent of ε. This *canard explosion* was discovered by Benoît et al. [7] and subsequently analyzed by Eckhaus [13], Dumortier and Roussarie [12], and others [23, 15].

Consider now another system with one slow and one fast variable:

$$\begin{aligned} \varepsilon \dot{x} &= y - x^2, \\ \dot{y} &= \mu - x + ay. \end{aligned} \tag{1.3}$$

This system also has a Hopf bifurcation, but it occurs when $x = \varepsilon a/2$, $y = \varepsilon^2 a^2/4$, and $\mu = \varepsilon a/2 - \varepsilon^2 a^3/4$. Its point of Hopf bifurcation is on the critical manifold but displaced from the fold by a distance that is $O(\varepsilon)$. When $a \neq 0$, the periodic orbits in the canard explosion of this system grow monotonically with variations of μ like those of system (1.2), but they become unbounded as μ varies over a finite interval. Whether the bifurcation is subcritical or supercritical is determined by the sign of a. When $a = 0$, the singular Hopf bifurcation at $\mu = 0$ is totally degenerate: system (1.3) has a family of periodic orbits that are level curves of the function $H(x, y) = \exp(-2y/\varepsilon)(y - x^2 + \varepsilon/2)$. In this case, the parabola $H = 0$ contains the stable and unstable slow manifolds of the system, and it bounds the family of periodic orbits.

The system (1.3) can be rescaled by $x = \varepsilon^{1/2} X$, $y = \varepsilon Y$, and $t = \varepsilon^{1/2} T$ to give

$$\begin{aligned} X' &= Y - X^2, \\ Y' &= \varepsilon^{-1/2}\mu - X + \varepsilon^{1/2} aY. \end{aligned} \tag{1.4}$$

This system can be transformed to the Hopf normal form

$$\begin{aligned} r' &= \frac{\varepsilon^{1/2} a}{16\sqrt{1 - \varepsilon a^2}} r^3 + o(r^3), \\ \theta' &= \sqrt{(1 - \varepsilon a^2)} + o(r) \end{aligned} \tag{1.5}$$

at the equilibrium.

System (1.3) is representative of generic singular Hopf bifurcations [2, 3, 8, 25] with one slow and one fast variable. There are three aspects of the bifurcation that are directly influenced by multiple time scales:

- The bifurcation occurs at a distance that is $O(\varepsilon)$ from a fold point.
- The periodic orbits emanating from the Hopf bifurcation undergo a canard explosion.
- The slow stable and unstable manifolds of the system cross each other as a varies.

Tangential intersections of the slow stable and unstable manifolds are not bifurcations in traditional terms, but rather a degeneracy in the slow-fast decomposition of the system [15] comparable to a homoclinic/heteroclinic bifurcation. Generically, such tangencies occur at different parameter values from those where the equilibrium point is on a fold curve or at the Hopf bifurcation parameter value. The crossing marks the transition from parameters at which the slow stable manifold converges to the equilibrium or periodic orbit and parameters for which it jumps along the fast direction after approaching the vicinity of the equilibrium. This transition is one of the most significant changes in dynamical behavior associated with the singular Hopf bifurcation.

Singular Hopf bifurcations with two slow variables and one fast variable are analogous to system (1.3) with a single slow variable. There are counterparts to each of the three properties listed above. Equilibrium points of a system with two slow variables lie on its two dimensional critical manifold. The folds of the critical manifold form a curve. A stable equilibrium point of the system (1.1) may approach and cross the fold curve in a generic manner when a single parameter is varied. If it does so, Hopf bifurcation occurs at a distance $O(\varepsilon)$ from the fold curve. Canard explosions also occur, but the dimension of the state space is now large enough to allow period-doubling and torus bifurcations as the periodic orbits grow. Section 3 gives examples of each of these bifurcations. In systems with two slow variables and one fast variable, the slow stable and unstable manifolds are each two dimensional and therefore can intersect transversally along a trajectory in the three dimensional state space. These intersections occur for open sets of parameters and are a common feature of systems near singular Hopf bifurcations. The location of the slow stable and unstable manifold intersections helps determine whether there are bounded attractors near the singular Hopf bifurcation.

This paper explores the dynamics of singular Hopf bifurcation via analysis of normal forms. Coordinate changes and scaling suggest a normal form analogous to (1.3), but the normal form has four coefficients that cannot be scaled to fixed values. If these coefficients are regarded as parameters (or *moduli*), then degenerate Hopf bifurcations occur in the system for some values of these coefficients. Regarding one of the coefficients as a second parameter, the theory of codimension two bifurcations [18] can be used to investigate the dynamics. In some cases, higher order terms in ε must be retained in a rescaled normal form to obtain nondegeneracy of the codimension two bifurcations.

Singular Hopf bifurcation with two slow variables has been studied previously in other papers [3, 8, 25, 27]. The normal form used by Braaksma [8] differs from the one used here: one difference is that Braaksma's normal form has "global returns" of trajectories that leave the vicinity of the equilibrium point in the flow. System (1.2) also has global returns but just one slow variable. This paper emphasizes the role of singular Hopf bifurcation in the creation of certain types of mixed-mode oscillations (MMOs). MMOs are oscillations in which there are small and large amplitude cycles in each period of the oscillation. Singular Hopf bifurca-

tions produce small oscillations near the equilibrium point that can be combined with global returns to create MMOs. MMOs appear to have been studied first in chemically reacting systems [4, 5, 22, 27] and then in lasers [21]. More recently, MMOs have been studied in neural oscillations [9], where they are sometimes associated with folded nodes [31, 33, 17] as well as singular Hopf bifurcations. Some of the subsidiary bifurcations analyzed here have been observed in the models of chemical oscillators, but their relationship to singular Hopf bifurcation does not seem to have been noticed previously. Section 4 discusses the "autocatalator" model analyzed by Petrov, Scott, and Showalter [28] and Milik and Szmolyan [27].

2. Coordinate changes and normal forms. The goal of this section is to derive a normal form for a generic system with two slow variables and one fast variable with an equilibrium point that crosses a simple fold transversally. We denote x as the fast variable and (y, z) as the slow variables. The fast equation for such a system near a simple fold can be reduced to $\varepsilon\dot{x} = y - x^2$ [1], perhaps using a rescaling of time. This is our starting point for deriving a normal form for singular Hopf bifurcation. We approximate the system by truncating nonlinear terms in the Taylor series expressions for $\dot{y}$ and $\dot{z}$. The truncated system is further reduced by noting that if $\dot{y} = \alpha + \beta x + \gamma y + \delta z$, then replacing z by $w = \alpha + \gamma y + \delta z$ makes $\dot{y} = \beta x + w$ while $\dot{w}$ is still an affine function of (x, y, z). We relabel w as z. Hopf bifurcation occurs when $\beta < 0$. Rescaling (x, y, z, t) by $(|\beta|^{1/2}, |\beta|, |\beta|^{3/2}, |\beta|^{-1/2})$ makes a further reduction to the case that $\beta = -1$. These coordinate transformations yield a truncated system of the form

$$\begin{aligned} \varepsilon\dot{x} &= y - x^2, \\ \dot{y} &= z - x, \\ \dot{z} &= -\mu - ax - by - cz. \end{aligned} \tag{2.1}$$

Note that a detailed study of higher degree normal forms for singular Hopf bifurcation with two slow variables does not appear in the literature. The term singular point is used in Arnold et al. [1] to refer to folded singularities [15] (pseudosingularities in Benoît [6]) that are regular points of the vector field (1.1) when $\varepsilon > 0$. A final rescaling $(x, y, z, t) = (\varepsilon^{1/2}X, \varepsilon Y, \varepsilon^{1/2}Z, \varepsilon^{1/2}T)$ and $(A, B, C) = (\varepsilon^{1/2}a, \varepsilon b, \varepsilon^{1/2}c)$ eliminates ε from the system:

$$\begin{aligned} X' &= Y - X^2, \\ Y' &= Z - X, \\ Z' &= -\mu - AX - BY - CZ. \end{aligned} \tag{2.2}$$

Our numerical studies and bifurcation analysis will be conducted largely with system (2.2). Note that A, B, and C tend to zero as $\varepsilon \to 0$ and that B tends to zero faster than A and C. The extent to which nonlinear terms in the equations for $\dot{y}$ and $\dot{z}$ that have order $\varepsilon^{1/2}$ following rescaling influence the dynamics described in this paper has not been investigated.

The "desingularized" slow flow of system (2.1) is

$$\begin{aligned} \dot{z} &= -2x(\mu + ax + bx^2 + cz), \\ \dot{x} &= z - x. \end{aligned} \tag{2.3}$$

This equation is obtained from (2.1) by setting $\varepsilon = 0$, differentiating the resulting equation $y - x^2 = 0$ to obtain $\dot{y} = 2x\dot{x}$, then eliminating $\dot{y}$ from the second equation and finally rescaling the equation by $2x$.

3. Normal form dynamics and flow maps. This section investigates the dynamics of the systems (2.1) and (2.2). As μ varies near zero in system (2.1), the equilibrium point crosses the fold curve of the critical manifold at the origin. This crossing has been called a *folded saddle-node type* II by Milik and Szmolyan [27] because the slow flow (2.3) has a degenerate equilibrium point at this parameter value. The bifurcation in the slow flow is a transcritical bifurcation. The origin is always a folded singularity (or pseudosingularity) that is a saddle when $\mu < 0$, a node when $0 < \mu < 1/8$, and a focus when $1/8 < \mu$. While the folded saddle-node appears as the main change in the dynamics of the slow flow, Hopf bifurcations of the systems (2.1) and (2.2) typically occur at nonzero values of μ. The equilibrium point of system (2.1) undergoes Hopf bifurcation at a value of μ that is $O(\varepsilon)$. Much of the analysis in this section is devoted to exploring this Hopf bifurcation and the family of periodic orbits emerging from it.

3.1. Hopf bifurcation. Equilibria of system (2.2) occur at points (X_e, X_e^2, X_e) with $\mu = -AX_e - BX_e^2 - CX_e$. The Jacobian at this equilibrium is the matrix

$$\begin{pmatrix} -2X_e & 1 & 0 \\ -1 & 0 & 1 \\ -A & -B & -C \end{pmatrix},$$

whose characteristic polynomial is

$$P(s) = s^3 + (C + 2X_e)s^2 + (B + 2X_eC + 1)s + (A + 2X_eB + C).$$

Thus Hopf bifurcation of the system occurs where $(B + 2X_eC + 1) > 0$ and

$$(C + 2X_e)(B + 2X_eC + 1) = (A + 2X_eB + C).$$

Note that $(B+2X_eC+1) > 0$ is satisfied when B and C are small. Thus, the Hopf bifurcation locus of system (2.2) is parametrized by the equations

$$\begin{aligned} A &= BC + 2X_eC^2 + 4X_e^2C + 2X_e, \\ \mu &= -AX_e - BX_e^2 - CX_e \end{aligned} \tag{3.1}$$

in terms of the equilibrium position X_e and the parameters B, C. If $B = 0$, then $A = 2X_eC^2 + 4X_e^2C + 2X_e$ and $\mu = -(2X_eC^2 + 4X_e^2C + 2X_e + C)X_e$. Since B is $O(\varepsilon)$ while A and C are $O(\varepsilon^{1/2})$, zero eigenvalues of the equilibrium occur near the origin only if $a + c$ is small in system (2.1).

The program Maple [26] has been used to compute the Hopf normal form of system (2.2). Consider first the case $B = 0$. System (2.2) can then be transformed to its Hopf normal form by rational coordinate changes if A, C, and μ are parametrized by X_e and ω, the magnitude of its imaginary eigenvalue. Whether the bifurcation is subcritical or supercritical is determined

by the sign of the first Lyapunov coefficient.[1] Maple yields the following expression for the first Lyapunov coefficient:

$$4\,\frac{{X_e}^3\left(12\,\omega^2{X_e}^2-4\,{X_e}^2-2\,\omega^2+\omega^4+1\right)}{\left(1-2\,\omega^2+\omega^4+12\,\omega^2{X_e}^2-8\,{X_e}^2+16\,{X_e}^4\right)\left(16\,{X_e}^4-8\,{X_e}^2+24\,\omega^2{X_e}^2-2\,\omega^2+\omega^4+1\right)}.$$

Substituting $\omega = \sqrt{1+2X_eC}$ and $X_e = 1/8\,\frac{-2\,C^2-2+2\,\sqrt{C^4+2\,C^2+1+4\,CA}}{C}$ gives the first Lyapunov coefficient in terms of A and C. The first Lyapunov coefficient is divisible by A and the leading order term of its Taylor series is $A/4$. The leading order term in the expansion of μ at the Hopf bifurcation is $-A(A+C)/2$. Following the rescaling of (2.1), the first Lyapunov coefficient is $O(\varepsilon^{1/2})$ and the value of μ is $O(\varepsilon)$.

Interestingly, there is a second term in the first Lyapunov coefficient of system (2.2) that is $O(\varepsilon^{1/2})$ in the case that $B \neq 0$ even though B is $O(\varepsilon)$. The coordinate transformations to Hopf normal form are rational if the system is parametrized by ω, X_e, and r, the magnitude of the real eigenvalue. Maple computes the first Lyapunov coefficient as a rational function P/Q of r, X_e, and ω. The leading terms in the Taylor series expansion of P and Q as functions of A, B, and C are $16C^5(2B + A^2 + AC + 2B^2)$ and $64C^5(A + C)$, respectively. If A and C are $O(\varepsilon^{1/2})$ and B is $O(\varepsilon)$, the first Lyapunov coefficient is $\frac{A}{4} + \frac{B}{2(A+C)} + o(\varepsilon^{1/2})$. Thus, even though B has higher order than A and C in terms of ε, it plays a significant role in the dynamics associated with the Hopf bifurcations of system (2.2).

Two different ways in which the nondegeneracy conditions for the Hopf bifurcation can fail are that the real eigenvalue r vanishes and that the first Lyapunov coefficient vanishes. Both of these degeneracies occur for small values of the parameters (A, B, C). When $r = 0$, a codimension two saddle-node Hopf bifurcation occurs if appropriate nondegeneracy conditions are met. The first Lyapunov coefficient vanishes along a surface in the parameter space that is asymptotic to $B = -A(A + C)/2$ as $\varepsilon \to 0$. This produces a *generalized* Hopf bifurcation, first analyzed by Bautin. The saddle-node Hopf and generalized Hopf bifurcations of system (2.2) are discussed in the next two subsections.

3.2. Saddle-node Hopf bifurcations. Saddle-node Hopf bifurcations (also called fold-Hopf bifurcations) occur at equilibria with both a zero eigenvalue and a pair of pure imaginary eigenvalues. The parameter values for which system (2.2) has such an equilibrium are given by $A = C(B - 1)$ and $\mu = BC^2/4$. Alternatively, these can be expressed by the equations $B = (A + C)/C$ and $\mu = C(A + C)/4$. Since B is of higher order than A and C in ε, these bifurcations are located where $A \approx -C$.

The truncated normal form of the saddle-node Hopf bifurcation [18] can be written in polar coordinates as

$$\begin{aligned}\dot r &= a_1 r z,\\ \dot z &= b_1 r^2 + b_2 z^2,\\ \dot\theta &= \omega.\end{aligned}$$

[1]The magnitude of the first Lyapunov coefficient depends upon the coordinates used in the eigenspace of the pure imaginary eigenvalues. Guckenheimer and Holmes [18] and Kuznetsov [24] use different coordinate systems that yield expressions which differ by a factor of 2. The expression here follows the conventions of Guckenheimer and Holmes [18].

The three coefficients a_1, b_1, b_2 determine the main features of the dynamics of its unfolding, for example, whether invariant tori occur close to the bifurcation. Maple calculations yield the expressions $\omega = 1 + B - C^2$ and

$$a_1 = \frac{C^2 - 1}{\omega^2},$$
$$b_1 = \frac{-B}{2\omega^2},$$
$$b_2 = \frac{-2B}{\omega^2}.$$

If $B > 0$, then all of these coefficients are negative, while if $B < 0$, then a_1 is negative and b_1, b_2 are both positive. Since $|b_i| < |a_1|$, these correspond to the cases IVb and III of Guckenheimer and Holmes [18, section 7.4]. Small invariant tori and chaotic solutions occur in generic unfoldings of case III.

3.3. Degenerate Hopf bifurcations. Hopf bifurcations are degenerate when their first Lyapunov coefficient vanishes [24]. Takens [32] described the unfolding of codimension two degenerate Hopf bifurcations, assuming that the second Lyapunov coefficient does not vanish. In the unfolding, the Hopf bifurcation makes a transition between subcritical and supercritical and there is a region with two periodic orbits that annihilate each other in a saddle-node of limit cycles bifurcation [18].

To find parameters where degenerate Hopf bifurcation might occur, we express the first Lyapunov coefficient as a rational function of X_e, A, B, C. Denote its numerator by P. We then compute the resultant of P and the Hopf polynomial $BC + 2X_e + 4CX_e^2 + 2X_eC^2 - A$ as functions of X_e to obtain a polynomial $R_H(A, B, C)$ that vanishes at degenerate Hopf points:

$$\begin{aligned}
R_H(A,B,C) = 256\,C^2(&-12\,A^2B - 15\,B^2A^2 + 20\,C^5A + 16\,C^2A^2 + 76\,C^4A^2 + 92\,C^3A^3\\
&+ 36\,C^2A^4 + 8\,C^7A + 16\,C^6A^2 + 8\,C^5A^3 + 8\,CA^3 + 16\,C^2B + 56\,BC^6\\
&+ 54\,C^4B - 120\,C^4B^2 - 65\,C^2B^2 + 36\,C^4B^5 + 91\,C^2B^4 + 8\,C^4B^3\\
&- 26\,C^6B^3 - 10\,C^4B^4 - 85\,C^6B^2 - 10\,C^8B^2 + 46\,C^2B^3 + 4\,B^2C^{10}\\
&- 32\,B^3C^8 + 55\,C^6B^4 + 26\,C^8B + 4\,C^{10}B + 8\,C^3A - 24\,B^2 - 24\,B^3\\
&+ 100\,C^3BA^3 - 144\,C^5B^3A - 124\,CB^3A - 156\,CB^2A + 22\,C^2BA^2\\
&- 32\,C^2B^3A^2 - 64\,CA^3B^2 + 60\,C^3B^4A + 76\,C^7AB - 52\,BCA^3\\
&+ 50\,BC^6A^2 + 4\,C^9AB - 95\,C^4B^2A^2 + 172\,C^3B^3A - 170\,C^3B^2A\\
&- 244\,C^5B^2A\\
&+ 128\,C^3BA + 148\,C^5BA + 4\,BCA + 192\,C^4BA^2\\
&- 210\,C^2B^2A^2 + 14\,C^7B^2A).
\end{aligned}$$

The leading order terms of $R_H(A, B, C)$ are

$$-1024\,C^2B\left(6\,B + 3\,A^2 - CA + 6\,B^2 - 4\,C^2\right),$$

implying that $B \approx (A+C)(4C-3A)/6$ at degenerate Hopf points with (A,B,C) small. For example, two approximate solutions of $R_H(A,B,C) = 0$ are $(-0.01, 0.00013335, 0.02)$ and $(-0.01, 0.00005, 0.02)$.

3.4. Periodic orbits. When $A = B = 0$ but $C \neq 0$, the family of periodic orbits at $\mu = 0$ is normally hyperbolic. Normal hyperbolicity implies that this surface of periodic orbits in (X, Y, Z, μ) space deforms but does not disappear when A and/or B are perturbed from zero. For most values of the parameters, the periodic orbits are isolated in the (X, Y, Z) state space. Continuation methods implemented in AUTO [11] and MATCONT [10] track the periodic orbits and locate saddle-node, period-doubling, and torus bifurcations as a single parameter is varied. Continuation methods further track curves of these bifurcations as two parameters are varied. This subsection presents some results obtained with MATCONT. Numerical integration has been used to check these continuation calculations and visualize complex trajectories from the family (2.2).

The first Lyapunov coefficient of the Hopf bifurcation in system (2.2) is $\frac{A}{4} + \frac{B}{2(A+C)} + o(\varepsilon^{1/2})$. When the first Lyapunov coefficient is negative, the bifurcation is supercritical, and stable periodic orbits emerge from the equilibrium. The periodic orbits can bifurcate as they grow in amplitude. Figure 1 shows four periodic orbits at the beginning of a period-doubling cascade computed with $(A,B,C) = (-0.05, -0.01, 0.1)$ and μ taking the values 0.0082, 0.0084, 0.0086, and 0.008618. As μ increases, three period-doubling bifurcations give successive transitions from the blue orbit to the green, then the red, and finally the thin blue orbit. The Hopf value of μ for these values of (A,B,C) is approximately 0.0008. Figure 2 shows a cross-section (green) to a quasi-periodic trajectory (blue) with parameter values $(A,B,C,\mu) = (-0.08, 0, 0.1, 0.001)$.

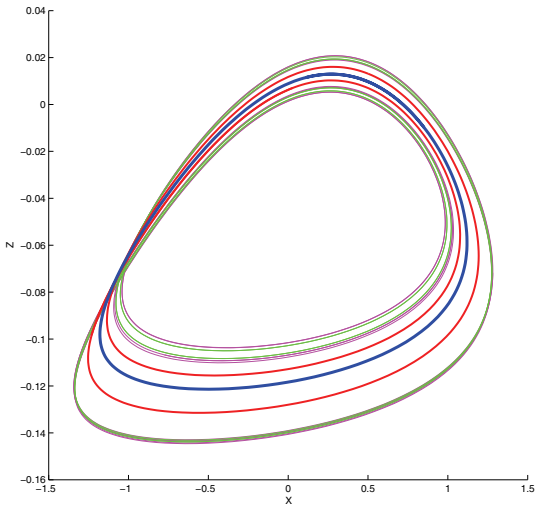

Figure 1. *Four periodic orbits of system (2.2) at the beginning of a period-doubling cascade, projected onto the (X,Z) plane. The heavy blue periodic orbit undergoes a period-doubling bifurcation to give rise to the red orbit. Two further period-doubling bifurcations yield the thin green and magenta. Parameter values are $(A,B,C) = (-0.05, -0.01, 0.1)$ and $\mu = 0.0082, 0.0084, 0.0086, 0.008618$ for the successive orbits.*

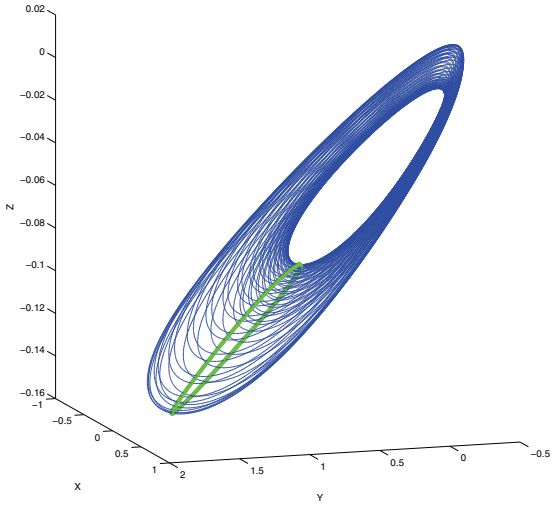

Figure 2. *A cross-section to a quasiperiodic trajectory of system (2.2). Parameter values are* $(A, B, C, \mu) = (-0.08, 0, 0.1, 0.001)$. *A portion of the trajectory is drawn as a blue curve. Intersections of the full computed trajectory with the plane* $X = 0$ *with* X *increasing are plotted in green.*

Figure 3 shows a bifurcation diagram for periodic orbits that emerge from a Hopf bifurcation as μ varies with $(A, B, C) = (-0.09, 0, 0.1)$. In this figure, the maximum and minimum values of x of the periodic orbits are plotted as a magenta curve. Points of period-doubling and torus bifurcations along this branch are marked and labeled "PD" and "T." Since $B = 0$, the system has a single equilibrium point, and the amplitude of the periodic orbits continues to grow as μ increases. The calculations are inconclusive as to whether this family of periodic orbits extends to ∞. When $B \neq 0$, system (2.2) has a second equilibrium on its critical manifold. If $A + C \neq 0$, then the second equilibrium is at finite distance from the origin. It appears that homoclinic orbits to this equilibrium can terminate families of periodic orbits. If $A + C \neq 0$, then the second equilibrium of system (2.1) is at finite distance from the origin and does not play a role in the local behavior of the singular Hopf bifurcation.

Branches of period-doubling and torus bifurcations with varying μ and B were computed with MATCONT 2.3.3 [10] and are shown in blue and green in Figure 4. Low order resonances of the torus bifurcations are marked by red dots. The three that occur for values of $\mu < 0.03$ are labeled with the order of the resonance; the point labeled R2 is the intersection of the two curves. The curve of torus bifurcations has a sharp bend near $\mu = 0.1$, where MATCONT detects several resonances of different orders as well as a fold of torus bifurcations very close to each other along the branch. The location of these resonances is indicated by the red marker at the right side of the figure.

4. Invariant manifolds. Invariant slow manifolds lie within an $O(\varepsilon)$ neighborhood of normally hyperbolic critical manifolds of slow-fast systems [14]. In typical settings, invariant manifolds are not unique, but their distance from each other is $O(\exp(-c/\varepsilon))$ for a suitable $c > 0$. The critical manifold $y = x^2$ of system (2.1) is normally hyperbolic away from the fold

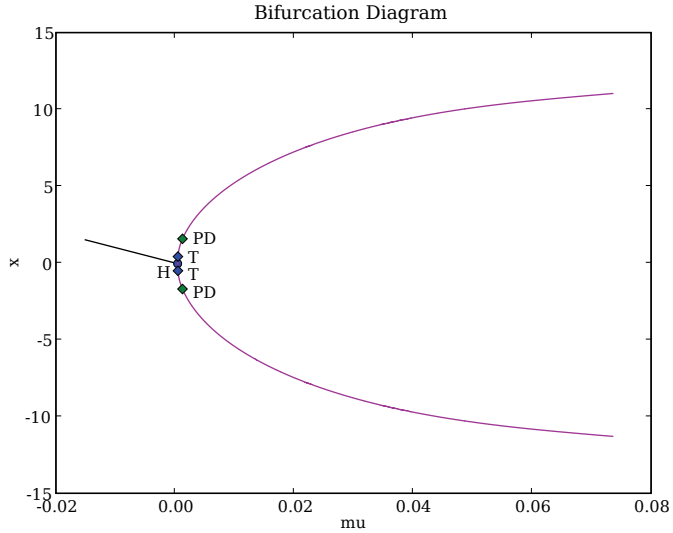

(a)

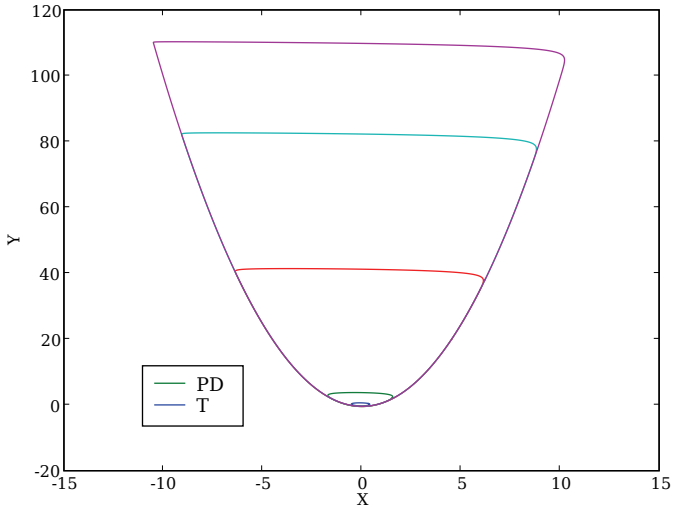

(b)

Figure 3. (a) *A bifurcation diagram showing the growth of periodic orbits emerging from a Hopf bifurcation (labeled "H") of system* (2.2) *as* μ *is varied. The maxima and minima of* X *along the periodic orbits are drawn as a magenta curve. Torus and period-doubling bifurcations along the family of periodic orbits are labeled "T" and "PD." The parameters* $(A, B, C) = (-0.09, 0, 0.1)$. (b) *Five periodic orbits within the family, including those at the torus and period-doubling bifurcations.*

curve $x = y = 0$, with a stable sheet in the half space $x > 0$ and an unstable sheet in the half space $x < 0$. The slow stable and unstable manifolds associated to these sheets of the critical

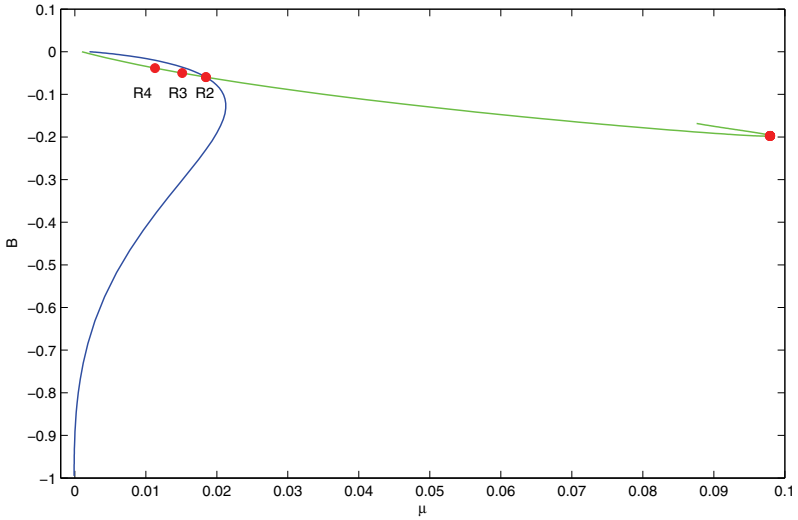

Figure 4. *Curves of torus and period-doubling bifurcations in a two dimensional slice of the parameter space with varying* (μ, B)*. The values of* A *and* C *are* 0.1 *and* -0.08*. The curve of torus bifurcations is drawn in green and points of second* (R2)*, third* (R3)*, and fourth* (R4) *order resonance are marked as red dots along the curve. Additional resonances occur near the red dot at the right-hand bend in this curve. The curve of period-doubling bifurcations is drawn in blue. The two bifurcation curves intersect at the point of second order resonance.*

manifold are important objects in the phase portrait of the system. Away from the critical manifold, the vector field is almost parallel to the x axis. The critical manifold and the slow stable and unstable manifolds separate trajectories on which x decreases rapidly from those on which x increases rapidly. The region of trajectories flowing from $x = +\infty$ to the stable slow manifold W_s^s is denoted M^-, and the region of trajectories flowing toward $x = -\infty$ from the unstable slow manifold W_s^u is denoted M^+. On the fast time scale, trajectories are drawn toward W_s^s and away from W_s^u. In many cases, parts of W_s^s and W_s^u lie on the boundary of the domain of attraction for bounded attractors. This section visualizes these manifolds, examining their intersections with each other and with the stable and unstable manifolds of the equilibrium.

4.1. Intersections of stable and unstable slow manifolds. Numerical investigations are more convenient with the rescaled system (2.2) than with system (2.1). The stable and unstable slow manifolds of system (2.2) lie close to the parabolic cylinder $Y = X^2$ for large values of $|X|$, though the theory does not specify how large. The stable slow manifold W_s^s is computed by forward numerical integration starting with initial conditions on a curve parallel to the Z axis with X suitably larger than $\sqrt{Y}$, while the unstable slow manifold W_s^u is computed by backward numerical integration starting with initial conditions on a curve parallel to the Z axis with X suitably smaller than $-\sqrt{Y}$. In the examples below, the initial conditions are chosen with $X = \pm 5$ and $Y = 10$. These trajectories approach W_s^s and W_s^u exponentially fast, so beyond a transient they give good approximations to the manifolds. Estimates for

how close the trajectories are to W_s^s and W_s^u can be obtained by comparing their distance from trajectories with initial conditions on the critical manifold since the critical manifold lies on the opposite side of the slow manifolds from the curves of initial conditions.

Figure 5(a) visualizes portions of the slow stable manifold W_s^s (blue) and the slow unstable manifold W_s^u (red) of system (2.2) as bundles of trajectories that begin on the lines $X = \pm 5$, $Y = 10$ until they reach $X = \mp 5$, $Y = 11$, or $T = 500$. Note that these stopping criteria extend the stable and unstable slow manifolds beyond the region where they lie close to the critical manifold. The parameter values used in Figure 5 are $(\mu, A, B, C) = (0, -0.05, -0.01, 0.1)$. The equilibrium is at the origin for these parameter values. It is on the fold curve and is stable with eigenvalues approximately $-0.0506, -0.0247 \pm 0.9934i$. The strong stable manifold of the equilibrium tangent to the eigenvector of its real eigenvalue is drawn in green. One branch of the strong stable manifold with X and Z negative approaches the slow unstable manifold while the other branch tends to ∞ in the X direction after its projection onto the (X, Y) plane makes a loop. The manifolds W_s^s and W_s^u appear to intersect transversally along a single trajectory Γ whose intersection with the plane $Z = X$ is depicted in Figure 5(b). In Figure 5(b), $Y' = Z - X = 0$ is the stopping criterion for the trajectories and piecewise

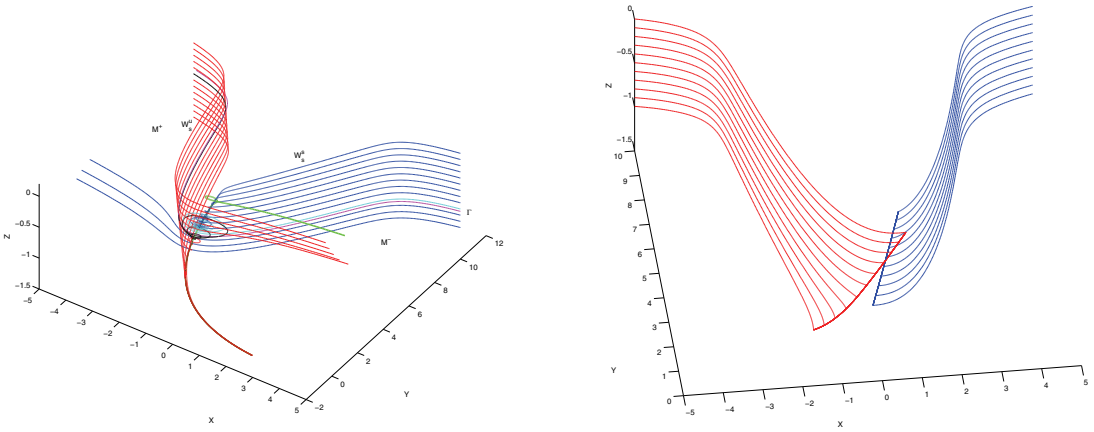

(a) (b)

Figure 5. (a) *Trajectories approaching and flowing along the slow stable manifold W_s^s are drawn in blue; trajectories approaching and flowing along the slow unstable manifold W_s^u are drawn in red. The initial conditions for these trajectories lie on the lines defined by $X = \pm 5$, $Y = 10$. The magenta curve approximates the intersection Γ of these two manifolds. The strong stable manifold of the equilibrium point is drawn in green. The equilibrium point is the forward limit set of the cyan trajectory and the dark blue trajectories above it. The blue trajectories below the magenta trajectory are unbounded, tending to $x = -\infty$ in finite time. Trajectories in the unstable manifold above the magenta trajectory tend to $x = +\infty$ as time decreases. The trajectories in the unstable manifold below the magenta trajectory tend to a branch of the strong stable manifold of the equilibrium which itself approaches the slow unstable manifold as time decreases. The slow unstable manifold W_s^u bounds the basin of attraction of the equilibrium point.* (b) *The same trajectories approaching W_s^s and W_s^u are drawn up to their intersection with the plane $Y' = Z - X = 0$. It is apparent that the intersection of these manifolds is transverse. The parameter values are $(\mu, A, B, C) = (0, -0.05, -0.01, 0.1)$.*

linear interpolations of the endpoints of these trajectories are drawn. An approximation to Γ is plotted as a magenta curve in Figure 5(a). Trajectories in W_s^s above Γ approach the equilibrium point, while trajectories below Γ tend to $-\infty$ along the X direction. The lowest trajectory in W_s^s above Γ is drawn in cyan to distinguish it from the others; the highest trajectory in W_s^u below Γ is drawn in black. In W_s^u, the trajectories above Γ tend to ∞ along the X direction while the trajectories below Γ spiral around the strong stable manifold of the equilibrium point. These observations motivate the conjecture that W_s^u is the boundary of the basin of attraction of the equilibrium point.

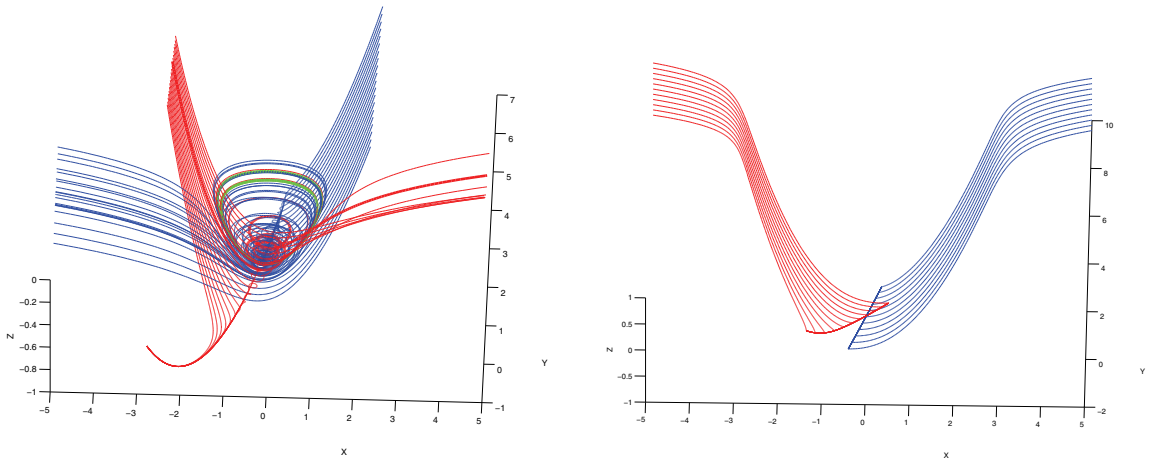

(a) (b)

Figure 6. (a) *Trajectories approaching and flowing along the slow stable manifold W_s^s are drawn in blue; trajectories approaching and flowing along the slow unstable manifold W_s^u are drawn in red. The initial conditions for these trajectories lie on the lines defined by $X = \pm 5$, $Y = 10$. A stable periodic orbit is drawn in green. All of the computed trajectories in W_s^s reach the plane $X = -5$ on their way to $X = -\infty$. The thick red trajectory shows that some of the trajectories in W_s^u that tend to $X = \infty$ oscillate before doing so.* (b) *The slow stable and unstable manifolds W_s^s and W_s^u intersect transversally. The parameter values are* $(\mu, A, B, C) = (0.0084, -0.05, -0.01, 0.1)$.

4.2. Intersections of the unstable slow manifold with the unstable manifold of the equilibrium point. As μ increases, the phase portraits of system (2.2) become more complicated. The equilibrium point has a supercritical Hopf bifurcation near $\mu = 0.0008$ and the periodic orbits born in this Hopf bifurcation enter a cascade of period-doubling bifurcations near $\mu = 0.008$, as illustrated in Figure 1. While μ increases, the asymptotic properties of the slow stable and unstable manifolds also change. Figure 6(a) visualizes portions of the slow stable (blue) and unstable (red) manifolds of system (2.2) as bundles of trajectories that begin on the lines $X = \pm 5$, $Y = 10$ and end on the plane defined by $Z' = 0$. The parameter values are $(\mu, A, B, C) = (0.0084, -0.05, -0.01, 0.1)$ used for the green period-doubled orbit displayed in Figure 1. This periodic orbit is also drawn in green here. As shown in Figure 6(b), the manifolds W_s^s and W_s^u intersect transversally, as they do when $\mu = 0$. However, in contrast to

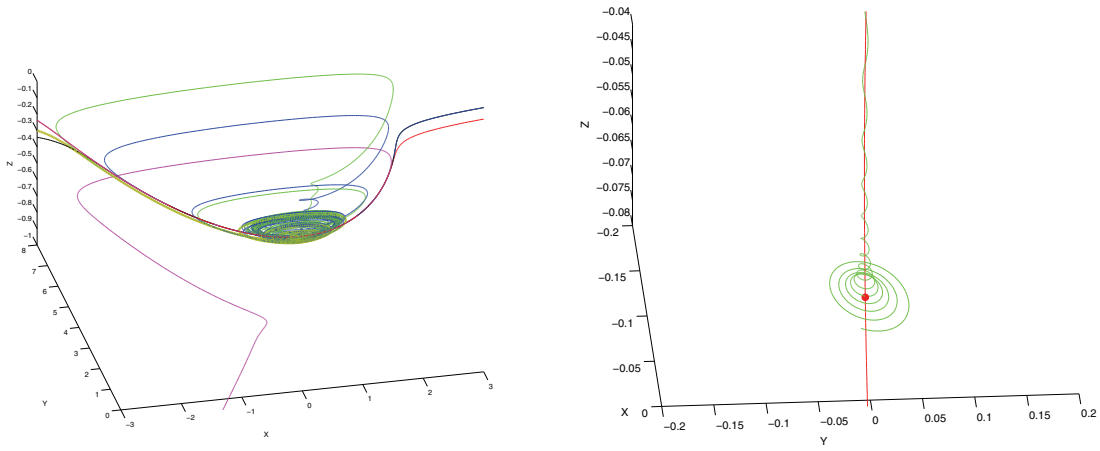

(a) (b)

Figure 7. (a) *Three pairs of trajectories for system* (2.2) *with parameter values* $(\mu, A, B, C) = (0.003686, -0.05, -0.01, 0.1)$. *The black and blue trajectories are forward trajectories that approach the slow stable manifold* W_s^s*; the magenta and red trajectories are backward trajectories that approach the slow unstable manifold* W_s^u*; and the olive and green trajectories are forward trajectories starting close to the unstable manifold of the equilibrium point. Note that the olive and green trajectories approach* W_s^u *but then diverge from it in opposite directions.* (b) *A detailed view showing how the green trajectory spirals around the red stable manifold of the equilibrium point before approaching the periodic orbit.*

the situation with $\mu = 0$, trajectories above the intersection in W_s^s escape the bounded region containing the periodic orbits, and some trajectories above the intersection in W_s^u oscillate before they tend to $X = \infty$. The dynamical events that produce these qualitative changes in W_s^s and W_s^u as μ increases from 0 to 0.0084 are hardly clear.

For values of μ slightly larger than the Hopf bifurcation value, the equilibrium is a saddle with a two dimensional unstable manifold W_p^u bounded by the periodic orbit. As μ increases, W_p^u begins to spiral around the periodic orbit as the eigenvalues of its return map become complex. Near $\mu = 0.003686$, it appears that W_p^u begins to intersect W_s^u, the unstable slow manifold. Figure 7 presents evidence for this intersection. Figure 7(a) plots three pairs of trajectories, each of which is separated by the slow manifolds. The black and blue trajectories are forward trajectories with initial conditions $(5, 10, -0.704948)$ and $(5, 10, -0.704947)$. The black trajectory lies below the intersection of W_s^s and W_s^u and flows to $X = -\infty$, while the blue trajectory turns back toward positive values of X and then appears to spiral around the stable manifold of the equilibrium point before approaching the periodic orbit. The magenta and red trajectories have initial conditions $(-5, 10, -0.291832)$ and $(-5, 10, -0.291831)$ and are followed backward. The magenta orbit lies below the intersection of W_s^s and W_s^u and flows backward to $X = -\infty$ while the red trajectory flows backward to $X = \infty$. The olive and green trajectories have approximate initial conditions $(-0.073363697, 0.005235108, -0.072670595)$ and $(-0.073363704, 0.005235153, -0.072670597)$, points that lie close to the unstable manifold of the equilibrium. These trajectories approach the unstable slow manifold W_s^u and follow it to near its intersection with $Y = 6$ before separating. The olive trajectory then tends to

$X = -\infty$ while the green trajectory follows a similar path as the blue trajectory, spiraling around the stable manifold of the equilibrium and then approaching the periodic orbit. One might conjecture that the equilibrium point has a homoclinic orbit for a value of μ close to 0.003686. Figure 7(b) shows the green trajectory spiraling around the red stable manifold of the equilibrium point in more detail. However, the close approach of the trajectory to the equilibrium point does not imply that the parameters are close to those with a homoclinic orbit. As explained by Guckenheimer and Willms [19], the stable manifold of the equilibrium may be transversally stable as one moves away from the equilibrium, and large volumes of the state space may flow close to the stable manifold. This example demonstrates that qualitative changes in the intersections of invariant manifolds for system (2.2) typically occur at different parameter values than those where there are local bifurcations of the equilibrium point or periodic orbits of the system.

4.3. Intersections of the stable slow manifold with the stable manifold of the equilibrium point. When the equilibrium point has a one dimensional stable manifold, intersections of that manifold with the slow stable manifold might be expected to occur as codimension one bifurcations. This section presents evidence for this bifurcation by examining parameters with $A = B = \mu = 0$ and $C > 0$. For these parameters, the equilibrium is at the origin, the plane $Z = 0$ is invariant under the flow and time reversible, and there is a family of periodic orbits surrounding the origin and bounded by the parabola $Y - X^2 = -1/2$ in the plane $Z = 0$. The orbits below this parabola are unbounded, tending to $X = -\infty$ in finite time as t increases and to $X = \infty$ as t decreases. The family of periodic orbits is normally hyperbolic: each orbit has a strong stable manifold consisting of trajectories that tend toward it as $t \to \infty$. Figure 8(a) shows a branch of the stable manifold of the origin for six values of C, namely $(0.01, 0.1002, 0.1004, 0.1006, 0.1008, 0.101)$. Figure 8(b) shows the intersection of the stable manifolds with the plane $X = 3$ for 51 equally spaced values in the C interval $[0.01, 0.0101]$. Figure 8(c) shows the intersections from a much finer mesh of 5001 parameter values in this interval. It is evident that the stable manifold W^s_p of the origin oscillates in the (X, Y) plane as Z increases. These oscillations cease and X tends to ∞ for values of Z that depend upon C. Since trajectories tend to ∞ in finite time, the values of (Y, Z) typically approach finite limits along W^s_p. However, there are values of C where these limits appear to jump. These are produced by small ranges of C in which W^s_p crosses W^s_s. Figure 8(d) visualizes one crossing. The intersection of W^s_p with the plane $Y = 3$ is plotted in red as C varies through a regular mesh of 11 points in the interval $[0.01000965, 0.01000975]$. As C varies in this interval, the intersections of W^s_s with the plane $Y = 3$, drawn as a set of 11 blue curves in Figure 8(d), hardly move. The three dimensional manifold in (X, Y, Z, C) space swept out by W^s_s and the surface swept out by W^s_p clearly intersect transversally. When A, B, and μ are perturbed so that the equilibrium point becomes a saddle, the transverse intersection persists.

4.4. Contrasts between systems with one and two slow variables. The figures of this section hardly begin a systematic analysis of the global bifurcations of the invariant manifolds of system (2.2). Since the system likely has chaotic attractors for some parameter values, a complete analysis does not seem feasible. The behavior displayed here contrasts with the simpler two dimensional flows of singular Hopf bifurcations in systems with one slow variable and one fast variable. There, the slow stable and unstable manifolds are each a single trajectory

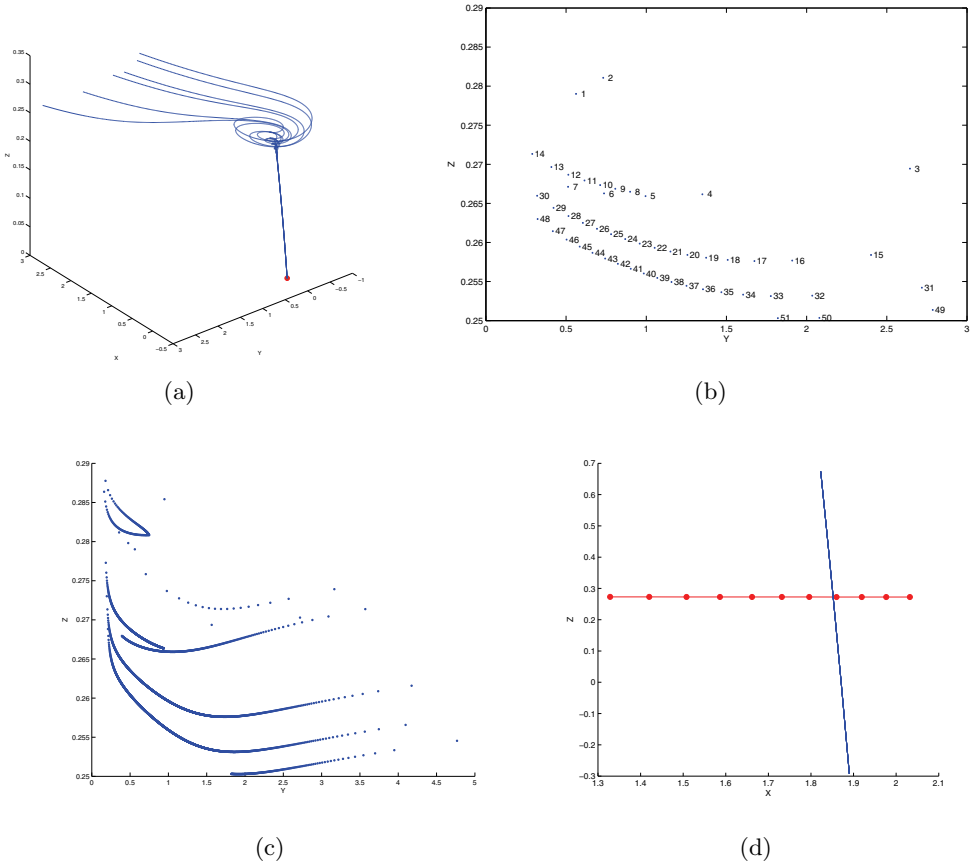

Figure 8. (a) *Trajectories lying in the stable manifold of the equilibrium point of system* (2.2) *for six different values of the parameter* C*:* $0.01, 0.1002, 0.1004, 0.1006, 0.1008, 0.101$*. The remaining parameters are zero.* (b) *Numbered intersections of the stable manifold of the equilibrium point of system* (2.2) *with the plane* $X = 3$ *for varying values of the parameter* C *in the interval* $[0.01, 0.0101]$*. Parameters* μ, A, B *are all zero.* (c) *Intersections from a mesh of* 5001 *parameter values in the interval* $[0.01, 0.0101]$*.* (d) *Intersections with the plane* $Y = 3$ *of the stable manifold of the equilibrium (red) for a mesh of* 11 *values of* C *in the interval* $[0.01000965, 0.01000975]$ *and intersections of the slow stable manifold (blue) with the plane* $Y = 3$*. There are* 11 *blue curves that are indistinguishable at this resolution.*

and the global bifurcation happens when the manifolds coincide. In the three dimensional setting investigated here, the slow stable and unstable manifolds are two dimensional and appear to intersect transversally in the vicinity of singular Hopf bifurcations. These intersections separate portions of the slow manifolds that turn in different directions. In some cases, parts of the manifolds become entangled with periodic orbits and the stable and unstable manifolds of the equilibrium. Sometimes the trajectories of these tangles remain bounded and sometimes they reemerge from the region of entanglement and proceed to $X = \pm\infty$. Further analysis of the intersections of these invariant sets is not pursued in this paper.

5. Mixed-mode oscillations in an example.

Mixed-mode oscillations (MMOs) have been observed and studied in chemical systems, for example, the Belousov–Zhabotinsky reac-

tion [20], and in the oxidation of carbon monoxide on platinum catalysts [22]. Several models have been proposed for these systems, but previous analysis has not identified that many of the properties seen in both the experimental data and models can be produced by singular Hopf bifurcations. Barkley [4] suggested that the minimum dimension of a system that fit the characteristics of MMOs in the Belousov–Zhabotinsky reaction was four. The more recent literature on MMOs in neural systems has focused upon MMOs produced by folded nodes [9, 30, 16], but some MMOs associated with singular Hopf bifurcations have characteristics that differ from those seen in the folded-node MMOs. Note that systems with singular Hopf bifurcations also have folded nodes, so singular Hopf bifurcations may produce MMOs that pass through folded nodes as well as ones that do not.

This section revisits one of the simplest models for MMOs—the autocatalator studied by Petrov, Scott, and Showalter [28] and Milik and Szmolyan [27]. The equations for this model are

$$\begin{aligned} \dot{a} &= \mu(\kappa + c) - ab^2 - a, \\ \varepsilon\dot{b} &= ab^2 + a - b, \\ \dot{c} &= b - c. \end{aligned} \tag{5.1}$$

In the studies of this system cited above, $\kappa = 2.5$ was held fixed and the parameters μ and/or ε were varied. The critical manifold of this system is given by $a = b/(1+b^2)$ and its fold curve is defined by $a = 1/2$, $b = 1$. At equilibrium points, $b = c$, so the equilibrium is on the fold curve when $b = c = 1$, $a = 1/2$, implying that $\mu = 1/(1+\kappa)$. In general, if we parametrize the equilibria of the system by c, then the curve of equilibrium points is given by $a = c/(1+c^2)$, $b = c$, $\mu = c/(c+\kappa)$. Computing the Jacobian of the system (5.1), we find that the criterion for Hopf bifurcation of the system is a polynomial expression that is affine in κ and quadratic in ε, so we can readily parametrize the Hopf bifurcation as a function of the variables c and ε. In addition to the equilibrium equations,

$$\begin{aligned} &\kappa_{hopf} \\ &= -\frac{c\left(9\,c^2\varepsilon + 2 - c^2 + 5\,\varepsilon + 6\,c^4\varepsilon + 5\,c^6\varepsilon^2 + 9\,c^4\varepsilon^2 + 7\,c^2\varepsilon^2 + 3\,c^6\varepsilon + 2\,\varepsilon^2 + c^8\varepsilon^2 + c^8\varepsilon - c^6\right)}{2 + 3\,c^4\varepsilon + 5\,c^6\varepsilon^2 + c^8\varepsilon^2 + 6\,c^2\varepsilon + 9\,c^4\varepsilon^2 + 7\,c^2\varepsilon^2 + 2\,c^6\varepsilon + c^8\varepsilon - c^2 + 4\,\varepsilon + 2\,\varepsilon^2 - c^6}. \end{aligned}$$

The function κ_{hopf} is singular at $c = 1, \varepsilon = 0$. For fixed κ, the Hopf criterion defines c as a smooth function of ε that vanishes at $c = 1$ and has slope $(3 + 2\kappa)/(1 + \kappa)$. Thus, there is indeed a singular Hopf bifurcation in this system. This does not appear in the analysis of Milik and Szmolyan [27] because they transform the parameters to set $\mu = \varepsilon\bar{\mu} + 1/(1+\kappa)$ and then use $\bar{\mu}$ and ε as the parameters they vary. In this representation, the Hopf bifurcations have parameter values that are close to $\bar{\mu} = 0.4375$ and are apparent as $\varepsilon \to 0$ only if $\bar{\mu}$ is also varied in the region near this Hopf value. Indeed, they do not analyze properties of the equilibrium point at all except at the values at which the Hopf bifurcation lies on the fold curve, a point termed a folded saddle-node in their work.

Petrov, Scott, and Showalter [28] studied the periodic orbits of system (5.1) using AUTO [11]. They work with two values of ε, namely, $\varepsilon = 0.01$ and $\varepsilon = 0.013$. For $\varepsilon = 0.013$, they observe that there is a supercritical Hopf bifurcation at $\mu \approx 0.29202$ and a second supercritical Hopf bifurcation at $\mu \approx 0.77372$. The first of these is the singular Hopf bifurcation: the

value of (a, b) is approximately $(0.49977, 1.031080)$. Petrov, Scott, and Showalter [28] observe that there is a narrow band of values of $\mu \in [0.297, 0.303]$ where the system has complex dynamics. The periodic orbits born at the singular Hopf bifurcation undergo a period-doubling cascade to a small amplitude chaotic attractor. Near $\mu = 0.29795$, the chaotic attractor disappears, and trajectories starting near the previous attractor approach a periodic MMO. Milik and Szmolyan use geometric and singular perturbation methods to study this system, producing return maps for some of the attractors. Figures 9 and 10 extend this analysis using the insights into the singular Hopf bifurcation described in this paper.

MMOs are formed from trajectories which concatenate small and large amplitude oscillations. In system (5.1), the large amplitude oscillations come from trajectories that pass "outside" the unstable slow manifold; i.e., they have larger values of a. To test whether trajectories with small amplitude oscillations flow to the outside of the unstable slow manifold, trajectories in the unstable manifold of the equilibrium were computed, similar to the calculations of the singular Hopf normal form illustrated in Figures 5, 6, and 7. Figures 9(a) and 9(b) display trajectories on the unstable manifold of the equilibrium point in blue and trajectories on the unstable slow manifold in red for parameter values $(\varepsilon, \kappa, \mu) = (0.013, 2.5, 0.2963)$ and $(\varepsilon, \kappa, \mu) = (0.013, 2.5, 0.2964)$, respectively. It appears that as μ increases from 0.2963 to 0.2964, the unstable manifold of the equilibrium point begins to intersect the unstable slow manifold. The intersection of these invariant manifolds seems to be intimately related to the formation of MMOs. Nonetheless, it is difficult to make definitive statements about these dynamics because the periodic orbits of the system have followed a period-doubling route to chaotic attractors for smaller values of μ, similar to the behavior displayed by the singular Hopf normal form (2.2) for parameters $(A, B, C) = (-0.05, -0.01, 0.1)$ and increasing μ (cf. Figure 1). Here, Petrov, Scott, and Showalter [28] showed that there are several families of MMOs as well as the small amplitude chaotic attractors in parameter ranges close to those displayed here.

Figure 9 suggests that intersections of the unstable slow manifold with the basins of small amplitude attractors are critical to the formation of MMOs. The value of ε used in this figure makes the system only moderately stiff. Figure 10 displays similar calculations for the smaller value $\varepsilon = 0.001$. Subfigure (a) shows trajectories in the unstable manifold of the equilibrium (blue) and the unstable slow manifold (blue) for $(\varepsilon, \kappa, \mu) = (0.001, 2.5, 0.2864)$. There is a stable periodic orbit, and this orbit forms the boundary of the unstable manifold of the equilibrium point. Subfigure (b) shows analogous information for $(\varepsilon, \kappa, \mu) = (0.001, 2.5, 0.2865)$. The stable periodic orbit persists, but some trajectories near the equilibrium point flow to the outside of the unstable slow manifold and generate MMOs. Figure 11 shows a portion of one of these MMOs as it passes close to the equilibrium point. The large amplitude excursions of the trajectory approach the stable manifold of the equilibrium point closely, and these are followed by slowly growing small amplitude oscillations similar to those that can appear in the aftermath of a subcritical Hopf bifurcation [19]. For these parameter values, the birth of MMOs is clearly the direct result of the intersections of the unstable slow manifold with the unstable manifold of the equilibrium.

6. Discussion. As a slow-fast system, the equations for singular Hopf bifurcation are reduced to a three dimensional vector field that can be rescaled so that the Hopf frequency

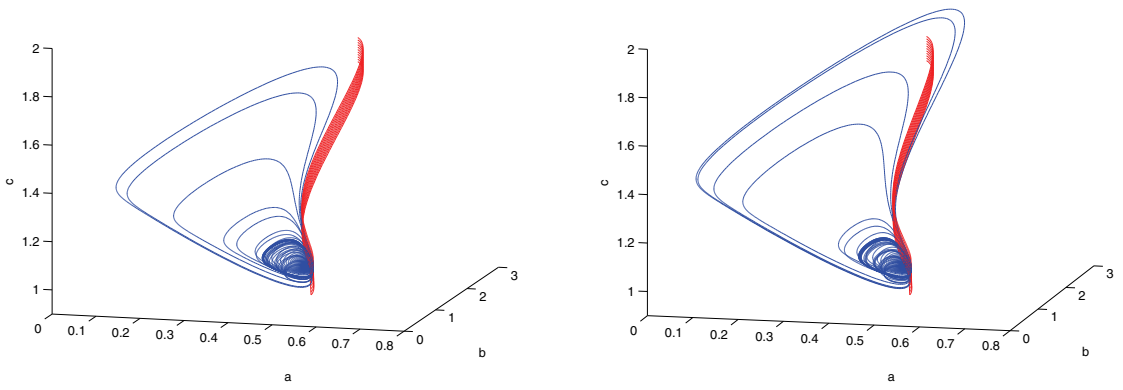

Figure 9. (a) *Trajectories on the unstable manifold of the equilibrium point (blue) and unstable slow manifold (red) of system* (5.1) *are drawn for* $(\varepsilon, \kappa, \mu) = (0.0013, 2.5, 0.2963)$. *The unstable manifold of the equilibrium point remains to the left side of the slow unstable manifold.* (b) *Analogous trajectories are drawn for* $(\varepsilon, \kappa, \mu) = (0.0013, 2.5, 0.2963)$. *Here the unstable manifold of the equilibrium point intersects the unstable slow manifold. Some trajectories with initial conditions near the equilibrium point make large excursions before approaching the small amplitude attractor.*

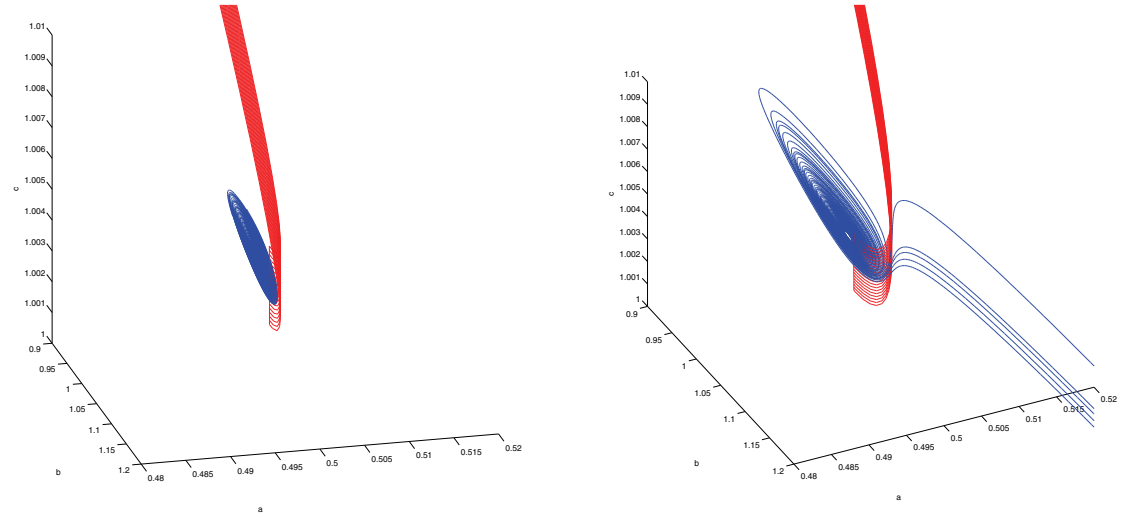

Figure 10. (a) *Trajectories on the unstable manifold of the equilibrium point (blue) and unstable slow manifold (red) of system* (5.1) *are drawn for* $(\varepsilon, \kappa, \mu) = (0.001, 2.5, 0.2864)$. *The unstable manifold of the equilibrium point remains to the left side of the slow unstable manifold and lies in the basin of attraction of a stable periodic orbit.* (b) *Analogous trajectories are drawn for* $(\varepsilon, \kappa, \mu) = (0.001, 2.5, 0.2865)$. *Here the unstable manifold of the equilibrium point intersects the unstable slow manifold. Some trajectories with initial conditions near the equilibrium point make large excursions and approach MMOs.*

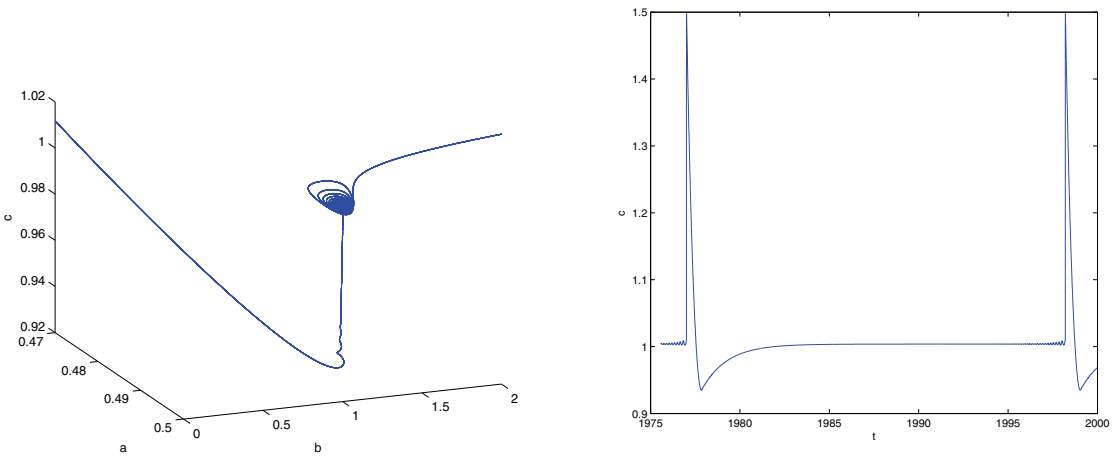

(a) (b)

Figure 11. (a) *A portion of an MMO trajectory of system* (5.1) *is drawn for* $(\varepsilon, \kappa, \mu) = (0.001, 2.5, 0.2865)$ *and initial condition* $(0.5, 1, 1)$. *The trajectory was computed to time* 2000, *and its intersections with a region around the equilibrium point were plotted for the time interval* $[1700, 2000]$. *The trajectory approaches the stable manifold of the equilibrium and flows out along its unstable manifold with slowly growing small amplitude oscillations before making another large excursion. The trajectory is approximately periodic, but the calculations do not conclusively rule out the possibility that there is a more complicated attractor that is very "thin."* (b) *The final cycle of the time series displaying the c coordinate of the trajectory displayed in subfigure* (a).

remains close to one as the singular perturbation parameter ε tends to zero. This scaling emphasizes the fast time scale whose singular limit is a vector field with an equilibrium point with pure imaginary and zero eigenvalues and a one parameter family of periodic orbits emanating from the equilibrium. Two coefficients of the Taylor expansion of the rescaled vector field, the real eigenvalue of its equilibrium and the first Lyapunov coefficient of its Hopf bifurcation, are $O(\varepsilon^{1/2})$. An interesting aspect of the normal form analysis is that an $O(\varepsilon)$ term in the Taylor expansion of the rescaled system still contributes to the first Lyapunov coefficient of the Hopf bifurcation at $O(\varepsilon^{1/2})$. The truncated normal form used in this paper includes this $O(\varepsilon)$ term. Thus the normal form has five parameters: the singular perturbation parameter, a primary parameter that drives the equilibrium point across the fold curve of the critical manifold, and three secondary parameters that can be regarded as moduli.

This paper highlights the complexity of Hopf bifurcation in multiple time scale systems with two slow variables and one fast variable. Numerical simulations and continuation calculations with the normal form demonstrate that periodic orbits near a singular Hopf bifurcation can have secondary bifurcations that produce quasiperiodic or chaotic trajectories of these systems in an $O(\varepsilon)$ neighborhood of the equilibrium undergoing Hopf bifurcation. The dependence of the secondary bifurcations on the moduli in the normal form is clearly very complicated. There are additional global bifurcations that separate parameter regimes with only small amplitude attractors from parameter regimes in which trajectories starting near the equilibrium can make large excursions. These transitions have been studied here by test-

ing for intersections of the two dimensional unstable manifold of the equilibrium point with the unstable slow manifold. From a pragmatic point of view, the boundary between trajectories that remain in the vicinity of the equilibrium point of the system and those that leave a neighborhood of the equilibrium point is an important aspect of the dynamics of singular Hopf bifurcation.

This paper is partly motivated by attempts to understand the mechanisms that create MMOs in slow-fast systems. MMOs have been observed in diverse physical systems and dynamical models. These MMOs appear to fall into different dynamical classes that have yet to be clearly delineated or analyzed. One class that has been identified and studied are MMOs associated with flow through a folded node [9, 16]. This paper identifies singular Hopf bifurcation as another mechanism for generating MMOs. As illustrated with the model chemical system (5.1), the intersections of the unstable slow manifold with the unstable manifold of a saddle-focus equilibrium point can produce MMOs. These intersections are a byproduct of singular Hopf bifurcation. The small oscillations of MMOs associated with singular Hopf bifurcation often begin with very small amplitude as they approach a saddle-focus equilibrium along its stable manifold and depart with growing oscillations along its unstable manifold. In contrast, the trajectories that pass through a folded node have oscillations that first decrease and then increase in amplitude. Figure 12 displays a trajectory of the system

$$\begin{aligned}\dot{x} &= y - x^2,\\ \dot{y} &= z - x,\\ \dot{z} &= -0.002\end{aligned}$$

with initial conditions $(50, 395, 0.16)$. The oscillations of this trajectory typify the small oscillations that one finds for MMOs produced by folded nodes. Compare this figure with Figure 11, showing an MMO associated with singular Hopf bifurcation in the autocatalator. In the normal form for the folded node, the numbers of oscillations with decreasing and increasing amplitude are equal. Further work to analyze the dynamical origins of MMOs from experimental observations of chemically reacting systems might be of interest [20]. It

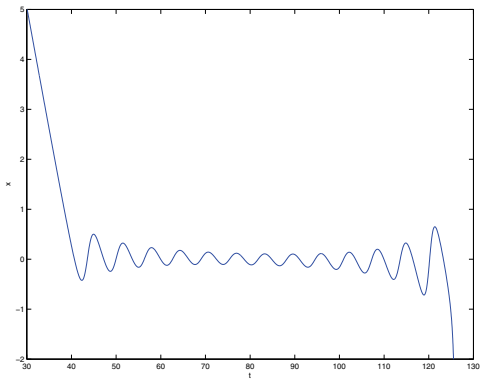

Figure 12. *Oscillations of a trajectory passing through a folded node.*

seems likely that MMOs associated with folded nodes and those associated with singular Hopf bifurcations both occur as well as MMOs that are far from these bifurcations.

REFERENCES

[1] V. I. Arnold, V. S. Afrajmovich, Yu. S. Il'yashenko, and L. P. Shil'nikov, *Dynamical Systems* V, Encyclopaedia Math. Sci., Springer-Verlag, Berlin, 1994.

[2] S. M. Baer and T. Erneux, *Singular Hopf bifurcation to relaxation oscillations*, SIAM J. Appl. Math., 46 (1986), pp. 721–739.

[3] S. M. Baer and T. Erneux, *Singular Hopf bifurcation to relaxation oscillations* II, SIAM J. Appl. Math., 52 (1992), pp. 1651–1664.

[4] D. Barkley, *Slow manifolds and mixed mode oscillations in the Belousov-Zhabotinskii reaction*, J. Chem. Phys., 89 (1988), pp. 3812–3820.

[5] D. Barkley, J. Ringland, and J. Turner, *Observations of a torus in a model of the Belousov-Zhabotinskii reaction*, J. Chem. Phys., 87 (1987), pp. 5547–5559.

[6] É. Benoît, *Canards et enlacements*, Inst. Hautes Études Sci. Publ. Math., 72 (1990), pp. 63–91.

[7] É. Benoît, J. L. Callot, F. Diener, and M. Diener, *Chasse au canards*, Collect. Math., 31 (1981), pp. 37–119.

[8] B. Braaksma, *Singular Hopf bifurcation in systems with fast and slow variables*, J. Nonlinear Sci., 8 (1998), pp. 457–490.

[9] M. Brøns, M. Krupa, and M. Wechselberger, *Mixed mode oscillations due to the generalized canard phenomenon*, in Bifurcation Theory and Spatio-Temporal Pattern Formation, Fields Inst. Commun. 49, AMS, Providence, RI, 2006, pp. 39–63.

[10] A. Dhooge, W. Govaerts, and Yu. A. Kuznetsov, *MATCONT: A MATLAB package for numerical bifurcation analysis of ODEs*, ACM Trans. Math. Software, 29 (2003), pp. 141–164. Also available online from http:// www.matcont.ugent.be/.

[11] E. Doedel, *AUTO: Software for Continuation and Bifuracation Problems in Ordinary Differential Equations*, http://indy.cs.concordia.ca/auto/.

[12] F. Dumortier and R. Roussarie, *Canard cycles and center manifolds*, Mem. Amer. Math. Soc., 121 (577) (1996).

[13] W. Eckhaus, *Relaxation oscillations, including a standard chase on French ducks*, in Asymptotic Analysis II, Lecture Notes in Math. 985, Springer-Verlag, Berlin, 1983, pp. 449–494.

[14] N. Fenichel, *Persistence and smoothness of invariant manifolds for flows*, Indiana Univ. Math. J., 21 (1971), pp. 193–225.

[15] J. Guckenheimer, *Bifurcations of relaxation oscillations*, in Normal Forms, Bifurcations and Finiteness Problems in Differential Equations, NATO Sci. Ser. II Math. Phys. Chem. 137, Kluwer, Dordrecht, The Netherlands, 2004, pp. 295–316.

[16] J. Guckenheimer, *Return maps of folded nodes and folded saddle-nodes*, Chaos, 18 (2008), 015108.

[17] J. Guckenheimer and R. Haiduc, *Canards at folded nodes*, Mosc. Math. J., 5 (2005), pp. 91–103.

[18] J. Guckenheimer and P. J. Holmes, *Nonlinear Oscillations, Dynamical Systems, and Bifurcations of Vector Fields*, Springer-Verlag, New York, 1983.

[19] J. Guckenheimer and A. Willms, *Asymptotic analysis of subcritical Hopf-homoclinic bifurcation*, Phys. D, 139 (2000), pp. 195–216.

[20] J. Hudson, M. Hart, and D. Marinko, *An experimental study of multiple peak periodic and nonperiodic oscillations in the Belousov-Zhabotinskii reaction*, J. Chem. Phys., 71 (1979), pp. 1601–1606.

[21] G. Kozyreff and T. Erneux, *Singular Hopf bifurcation to strongly pulsating oscillations in lasers containing a saturable absorber*, European J. Appl. Math., 14 (2003), pp. 407–420.

[22] K. Krischer, M. Lübke, M. Eiswirth, W. Wolf, J. L. Hudson, and G. Ertl, *A hierarchy of transitions to mixed mode oscillations in an electrochemical system*, Phys. D, 62 (1993), pp. 123–133.

[23] M. Krupa and P. Szmolyan, *Extending geometric singular perturbation theory to nonhyperbolic points—fold and canard points in two dimensions*, SIAM J. Math. Anal., 33 (2001), pp. 286–314.

[24] Yu. A. Kuznetsov, *Elements of Applied Bifurcation Theory*, 3rd ed., Appl. Math. Sci. 112, Springer-Verlag, New York, 2004.

[25] Y. Lijun and Z. Xianwu, *Stability of singular Hopf bifurcations*, J. Differential Equations, 206 (2004), pp. 30–54.
[26] http://www.maplesoft.com/.
[27] A. Milik and P. Szmolyan, *Multiple time scales and canards in a chemical oscillator*, in Multiple-Time-Scale Dynamical Systems (Minneapolis, 1997), IMA Vol. Math. Appl. 122, Springer-Verlag, New York, 2001, pp. 117–140.
[28] V. Petrov, S. Scott, and K. Showalter, *Mixed-mode oscillations in chemical systems*, J. Chem. Phys., 97 (1992), pp. 6191–6198.
[29] J. Rinzel, *A formal classification of bursting mechanisms in excitable systems*, in Proceedings of the International Congress of Mathematicians, Vols. 1, 2 (Berkeley, 1986), AMS, Providence, RI, 1987, pp. 1578–1593.
[30] J. Rubin and M. Wechselberger, *Giant squid—hidden canard: The 3D geometry of the Hodgkin-Huxley model*, Biol. Cybernet., 97 (2007), pp. 5–32.
[31] P. Szmolyan and M. Wechselberger, *Canards in R^3*, J. Differential Equations, 177 (2001), pp. 419–453.
[32] F. Takens, *Unfoldings of certain singularities of vector fields: Generalized Hopf bifurcations*, J. Differential Equations, 14 (1973), pp. 476–493.
[33] M. Wechselberger, *Existence and bifurcation of canards in $\mathbb{R}^3$ in the case of a folded node*, SIAM J. Appl. Dyn. Syst., 4 (2005), pp. 101–139.